

*Full Length Research Paper*

## Characterization of stainless steel SS-1672

Farah Noori<sup>1\*</sup> and Solveig Melin<sup>2</sup>

<sup>1</sup>Physics Science, Baghdad University, Baghdad, Iraq.

<sup>2</sup>Division of Mechanics, Lund University, Lund, Sweden.

Accepted 9 July, 2012

**This research concerns characterization of stainless steel SS-1672 with 0.46 wt.% carbon concentration, at room temperature with respect to mechanical properties and morphology. Specimens were divided into two groups according to heat treatment, and were hardened at three different temperatures (250, 450 and 650°C) to obtain different martensitic content. Hardness results are compared with those of the normalized condition and simulated by using the finite element method. The results show that hardness decrease with increasing martensitic content. Fatigue tests were performed and simulated by using the finite element method and fatigue life analyses by using the fatigue life prediction method in Ansys were carried out. One of the experiments survived  $10^6$  cycles at applied stress 241 MPa. This indicates the endurance limit,  $\sigma_e$ , to be slightly above 240 MPa. The microstructure observed by optical microscopic and scanning electron microscope (SEM) showed pearlite and martensite phases clearly distinguishable. Fractography studies also indicated the nature of typical fracture surfaces at low and high cycle fatigue.**

**Key words:** Fatigue [(Low Cycle Fatigue (LCF) and high cycle fatigue (HCF)], stainless steel, morphology, toughness of metallic alloys.

### INTRODUCTION

The mechanical resistance of engineering components to avoid failure in case of repeated loads is dependent on the material together with the type of loading and load level. Repeated stresses might lead to serious consequences in terms of failure due to fatigue. Mechanical fatigue is the dominant source of failure, causing about 90% of collapses in engineering components. The collapses due to fatigue occur under stress levels below collapses under static loading, therefore fatigue testing is a very important mechanical test to pay attention to. A fatigue related failure might occur suddenly without prior warning and the fatigue behavior interpreted by a traditional cycle diagram is useful (Robert, 2005; Yung et al., 2005).

In general, it has been observed that fatigue crack growth can be explained by growth or nucleation of small stage I fatigue cracks in slip bands or in grain boundaries. During repeated loading such cracks extends and crosses

nearby grain-boundaries to eventually line up perpendicular to the applied stress to become a stage II crack following the Paris law (Yung et al., 2005).

Many means for raising the capability of fatigue resistance have been developed, that is, cold rolling or different heat treatments such as annealing, quenching and tempering, depending on the type of application. Medium carbon steels can be used for manufacturing mechanical engineering parts, industrial, medical or civil (Eric, 2006). Case hardening steels are particularly suitable.

Research that address the failure of metals, with focus on the nature of the fatigue mechanisms of fracture, starting from crack initiation and the behavior during growth is thus of utter most importance. Here, the stainless steel SS-1672, which contains 46% carbon steel will be investigated. Two parameters controlling fatigue failure of steel are chemical composition and morphology. It is possible used of cold-rolled or subjected to heat treatment (annealing, quenching and tempering), depending on the application for which it is intended. It is commonly used for manufacturing

\*Corresponding author. E-mail: [farah.noori@scbaghdad.edu.iq](mailto:farah.noori@scbaghdad.edu.iq).

**Table 1.** Chemical composition of pearlite SS-1672 alloy.

Elements of alloy	C	Si	Mn	P	S
Wt. %	0.46	0.25	0.80	Max. 0.035	Max. 0.030

mechanical parts, such as clutches, springs, saws, valves, measuring tape. Case hardening steels are particularly suitable.

The suitable way to follow the fatigue test when designing is to understand the Wohler's curve of the material used. The Wohler's curve is known as the S-N curve which related between the stress (S) and number of cycles to failure (N). Two different regions are noticeable the high cycle fatigue in the right, has low stresses and elastic deformation corresponding to a high fatigue life and low cycle fatigue in the left, has high stress and plastic deformation and low fatigue life.

## EXPERIMENTAL WORK

### Material

Characterization of steel SS-1672 is performed with respect to tensile properties, fatigue properties, hardness and microstructure. The chemical composition of the material which examine with the optical emission spectrometer device is seen in Table 1 (Fagersta and Fagersta, 1962).

### Heat treatments

Hardness test specimens were manufactured with cylindrical shape with 1 cm diameter and 2 cm height. The specimens were heat treated before the hardness tests using a Linn Electro Them furnace, able to supply a maximum temperature of 1000°C.

For these experiments, the specimens were first heated to a temperature of 850°C and held there for a period of 15 min, where after they were quenched in cold water in order to obtain a transformation to a martinsite phase (Jaykant, 2009).

For tempering, the hardness specimens were heated for periods of 30 min at three different anneal temperatures; 250, 450 and 650°C, and in between the different anneal treatments, the specimens were cooled in air before tested. The tempering was done to remove internal stresses and to get different microscopic phases for the purpose of studying the hardness after each anneal treatment (Jaykant, 2009).

### Microstructure examination

Samples for microstructure examination with optical and scanning electron microscope were prepared. The specimens were cut in cylindrical shape with 7 mm diameter and 5 mm height, and to minimize the surface roughness, the samples were grinded using different grades of wet SiC papers; 120, 320, 500, 1200 and 2400 particles/inch, respectively, and finally polished on a rotating disc using a high performance diamond paste, DP-suspension, with a particle diameter of 3 µm. Grinding and polishing were performed using a Steruers Rotopol-2. It works by spreading a grind over the rotating disc and pressing the sample onto the spinning disc. Distilled water and alcohol were used in-between the grinding

operations to clean the samples. Etching with Nital (2% HNO<sub>3</sub>) immersion was carried out during a few seconds to be able to reveal different phases, followed by cleaning with water and alcohol.

## Mechanical properties tests

### Tensile test

One tensile test was performed. The specimen was manufactured according to the ASTM E8 recommendations (ASM handbook, 1996). The diameter of the specimen was 7 mm and nominal measuring length 10 cm. The specimen was after machining grained with SiC papers with 500 and 1200 particles/inch. The tensile test was executed at room temperature using an universal electronic digital Instron 8500 machine at an elongation speed of 2 mm/min. The Instron machine was calibrated before the test and the calibration curve is seen in Figure 1.

For the calibration, an extensometer was mounted on to a calibration specimen with a gap of 25 mm and the specimen was loaded by a force that was increased in steps and kept constant at each stress level to ensure that the stress level kept constant with time. Initially, the machine was unloaded for 12 s to ensure that no disturbances in the surrounding created a false signal. Thereafter, the following sequence of force levels was applied: 0.449, 1.000 and 1.495 kN during 8.5 s each. As seen from Figure 1, the drift is very slight.

### Fatigue testing

Six fatigue experiments were performed and the specimens were manufactured according to the ASTM E1823 recommendations (ASM handbook, 1996). The diameters of all specimens were 7 mm and nominal measuring length 3.5 cm. The specimens were prepared by grinding the surfaces with SiC papers with 500 and 1200 particles/inch. For the fatigue tests a MTS machine was used, applying sinusoidal loading with stress ratio  $R = \sigma_{min}/\sigma_{max} = -1$ , with  $\sigma$  denoting the amplitude of applied load as shown in Figure 2. All six tests were performed at room temperature at a frequency of 15 Hz. This choice of frequency ensured that no thermal softening of the material occurred.

### Hardness tests

Rockwell hardness tests conducted with two shapes of indenter for two groups of SS-1672 alloy specimens were performed: Test B (HRB) with a steel sphere with diameter 1/16 inch, indenting at a load of 100 kgf, and test C (HRC) with a 120° diamond cone at a load of 150 kgf. The hardness of each sample was read directly from the testing device.

## RESULTS AND DISCUSSION

### Tensile test

The tensile test was performed to characterize the tensile

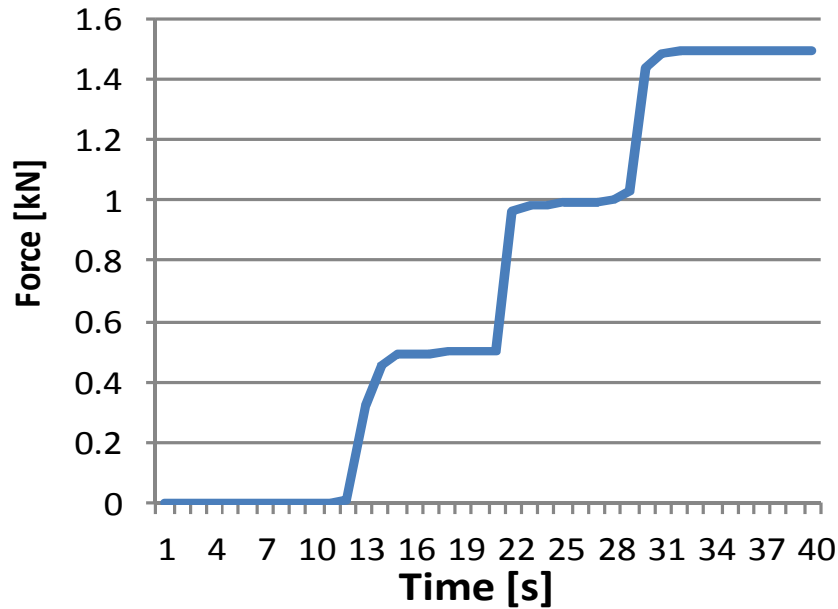


Figure 1. Calibration curve for Instron 8500.

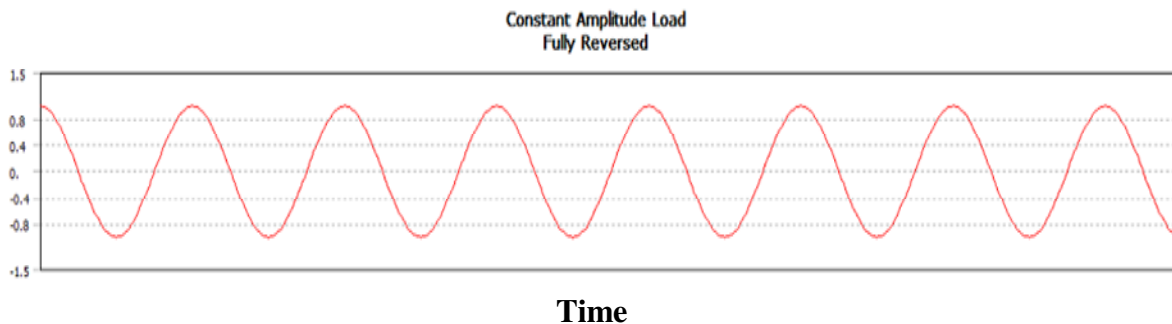


Figure 2. Normalized applied stress as function of time.

behavior of the SS-1672 alloy at room temperature, in addition to extract data from the elastic portion of the stress-strain curve to find proper load levels for the fatigue experiments. The stress-strain curve can be seen in Figure 3. From the tensile curve the yield stress,  $\sigma_y$ , the ultimate strength,  $\sigma_T$ , and the Young's modulus,  $E$ , were determined. Further, the relative elongation was determined as the difference between the specimen length before and after rupture, normalized by the original length. The contraction was determined as the ratio between the neck area after rupture and the initial specimen cross section area. In Figure 4, the specimen before and after rupture can be seen. The toughness was determined from the area under the stress-strain curve in Figure 4 as:

$$w = \int_0^{\epsilon_f} \sigma d\epsilon \quad (1)$$

with  $w$  denoting the toughness and  $\epsilon_f$  the strain upon failure. The result is  $w = 18.9 \text{ Nm/m}^3$ .

The values resulting from the tensile test are shown in Table 2. It was observed from Table 2 that the measured value of the mechanical properties as regards yield stress, ultimate strength, Young's modulus, relative elongation and contraction values of the test sample compared well with literature, cf. [7], material number 141650.

### Hardness tests

The results of the Rockwell HRB and HRC hardness tests are displayed in Table 3. The values in Table 3 refer to HRB hardness measures of the material before heat treatment and to HRC hardness measures of specimens after hardening heat treatment at 850°C to obtain a

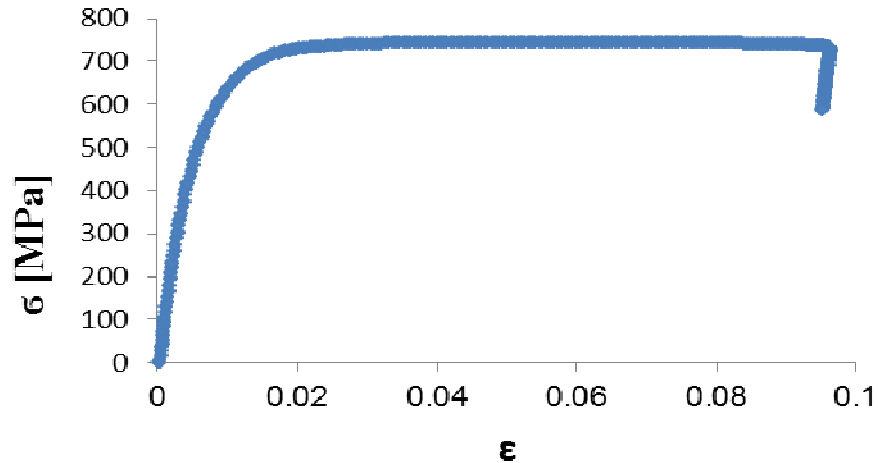


Figure 3. Stress as function of strain for SS-1672.



Figure 4. The tensile specimen before and after rupture.

Table 2. Tensile test results.

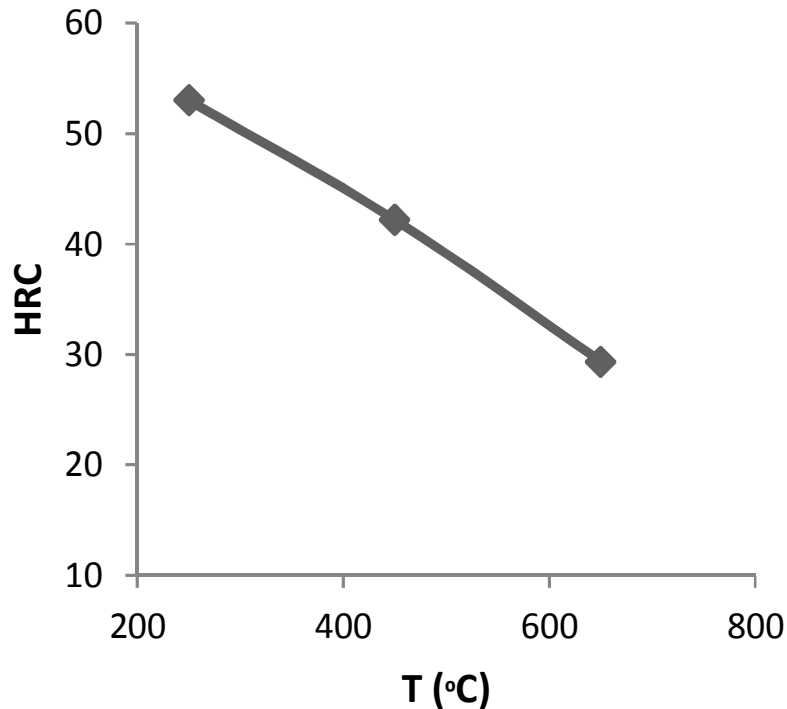
Mechanical properties	Literature [7]	Experimental
$\sigma_y$ MPa	860	742
$\sigma_T$ MPa	>550	594
E GPa	206	206
Relative elongation	9%	9%
Contraction	52%	53%

martensite phase. Martensite is a hard and brittle phase, while pearlite is a very soft and ductile phase. Therefore, it is logical to expect an increase in hardness in dual phase martensitic steel as the amount of the softer ferrite matrix is reduced.

Figure 5 shows the variation of HRC hardness of SS-1672 with tempering which consists of heating the hardened steel at different anneal temperatures below hardening temperature. The three measured values were connected by a fitting line using the least square method.

**Table 3.** The hardness test results.

Pearlite		HRB		Average
SS-1672	103.6	104.2	103.4	103.73
Martensite		HRC		Average
SS-1672	61	61.3	61.2	61.15

**Figure 5.** HRC as a function of anneal tempering temperature.**Table 4.** Maximum force applied maximum depth and residual depth.

	Experimental (HRC)	Simulation
Fmax	1470 N	1451 N
hmax	0.49 mm	0.50 mm
hc	0.47 mm	0.47 mm

It is observed that the hardness decreases with increasing tempering temperature due to the increasing ductility of the martensite phase induced by tempering. Tempering increases the resistance of the material to fracture and relieves the internal stresses.

The applied loads for the HRB test was 980 N and for the HRC test 1470 N. The maximum depth  $h_{max}$  and residual depth  $h_c$  after unloading was measured using a Reichert Austria with an accuracy of 0.01 mm. The results of the tests can be seen in Table 4.

### Hardness simulation

A simulation with the finite element program Abaqus is used to determine the relationship between the applied force at a diamond cone indenter and the displacement depth in the specimen together with the corresponding stress distribution. A von Mises (Ottosen and Ristinmaa, 2005) material model is used with material parameters taken from Table 2. The model is plane axisymmetric and the element type is 4 node linear square elements and in

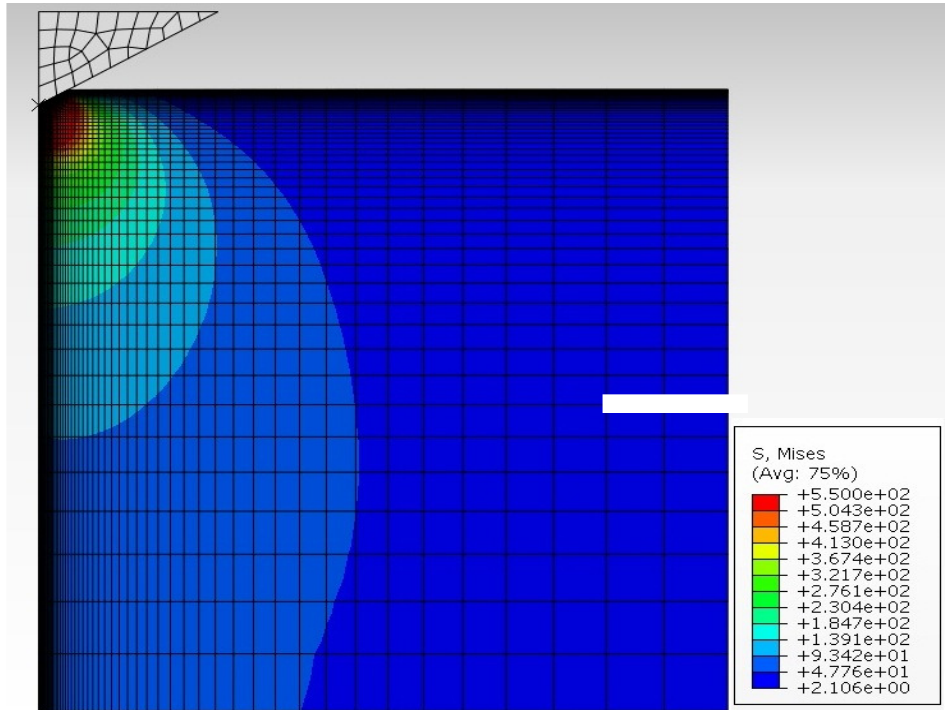


Figure 6. Stress distribution in the hardness specimen from FEM simulation.

Table 5. The stress levels and the number of cycles to failure.

Force level kN	Stress MPa	Number of cycles
21.9	640	543
19.6	546	1060
16.6	431	23049
14.6	348	94482
11.6	301	303084
8.9	241	>10E+6

all 5184 elements were used. The simulated test piece thickness should be at least 10 times the indentation depth (ISO, 2002), as empirically determined.

The exact limits of influence of the boundary conditions on the simulation depend on the geometry of the indenter used and the material properties of the specimen. In this case, the experimental value of  $h_{max} = 0.5$  mm, which means that the model height should be at least 5 mm. Here, the height 5 mm was chosen.

A stiff cone was pressed vertically into the sample in the simulation by applying a force along the symmetry line so that simulated values of  $h_{max}$  and  $h_c$  came to agree with the experimental results. The experimental and simulation data for maximum force  $F_{max}$ , maximum displacement depth  $h_{max}$  and residual depth  $h_c$  after removal of the applied load are shown in Table 4 for a HRC test for the material as received. It is seen that the agreement is very good.

Figure 6 shows a plot of the simulated stress distribution in the specimen. The yield stress is about 740 MPa according to Table 2, so the simulation predicts the effective plastic zone to extend 0.94 mm along the symmetry line if the yield stress is set equal to the von Mises stress. Thus the plasticity is well contained within the model.

### Fatigue tests

The fatigue tests were performed under six constant applied stress amplitudes with  $R = -1$  with test specimens from material as received. The stress levels and the number of cycles to failure at each test are seen in Table 5. One of the experiments survived  $10^6$  cycles at applied stress 241 MPa. This indicates the endurance limit,  $\sigma_e$ , to be around or slightly above 240 MPa. This agrees exactly

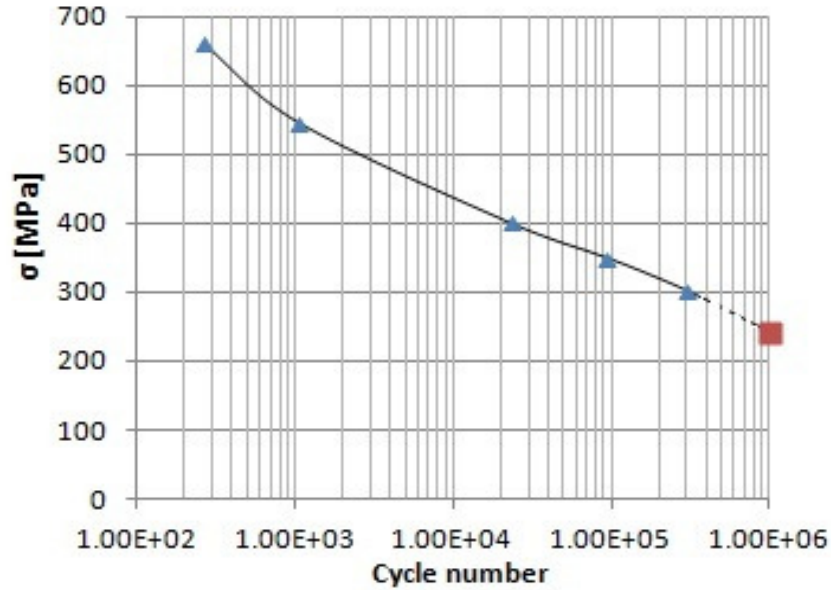


Figure 7. Stress levels as a function to number of cycles, ■ indicates the run-out test.

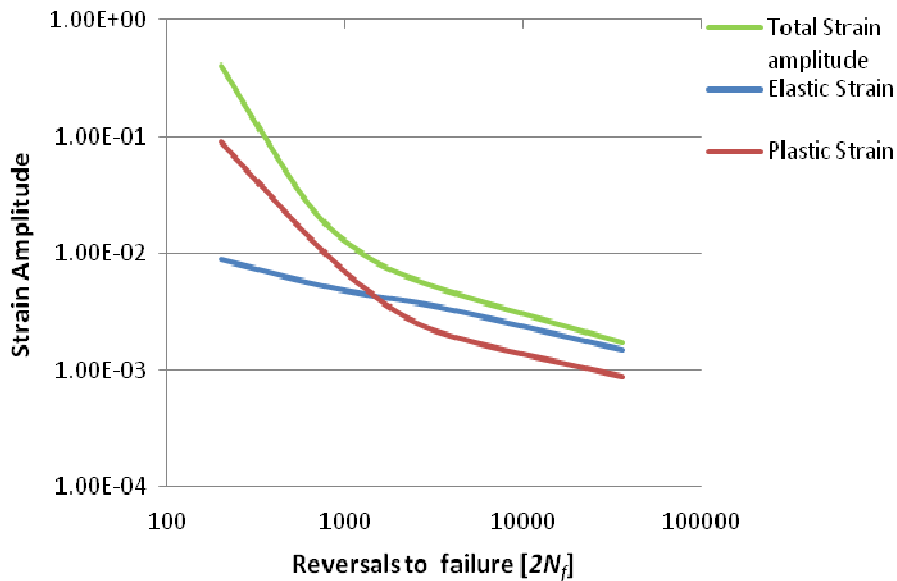


Figure 8. Strain amplitudes as a function of reversals to failure.

with  $\sigma_e$  taken from literature (Handbook in Solid Mechanics, 2008). The stress to number of cycles to failure is shown in Figure 7.

The process of failure is due to the progressively propagation of flaws and initiation of micro cracks under cyclic loading. The process is enhanced by the stress concentrations induced by at such flaws and cracks (Balbi et al., 2009).

**Analysis of the fatigue data**

The total strain as function of reversals to failure was approximated from the tensile test curve and agrees with the simulated curve from Ansys (FEM model). The total strain amplitude,  $\Delta\epsilon/2$ , as well as its elastic,  $\Delta\epsilon_e/2$ , and plastic,  $\Delta\epsilon_p/2$ , parts versus number of cycles to failure are shown in Figure 8. The elastic and plastic strain

Table 6. The marrow parameters.

Fatigue strength coefficient MPa ( $\sigma_f$ )	Fatigue ductility coefficient ( $\epsilon_f'$ )	Fatigue strength exponent (b)	Fatigue ductility exponent (c)
1154	0.18	-0.06	-0.53

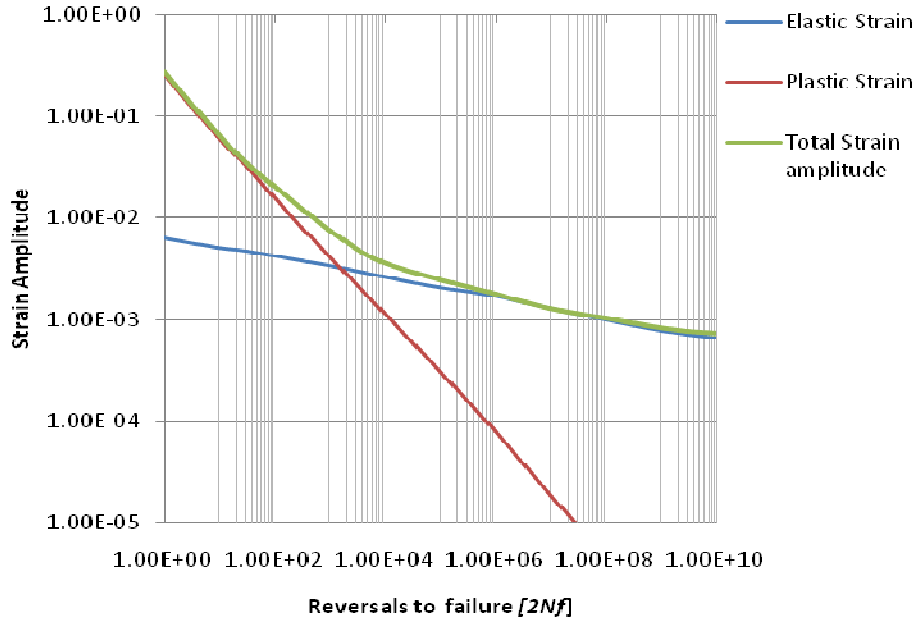


Figure 9. Total, elastic and plastic strain amplitudes as functions of reversals to failure with Excel.

amplitudes are determined from the total strain amplitude by using Equations (2) and (3) (Suresh, 2001; Chiu, 2005):

$$\Delta \epsilon_e = \frac{\Delta \sigma}{E} \tag{2}$$

$$\Delta \epsilon_p = \Delta \epsilon - \Delta \epsilon_e \tag{3}$$

**Fatigue simulation**

To determine the regions of high and low cycle fatigue, respectively, the transition point can be estimated from the Morrow relation:

$$\frac{\Delta \epsilon}{2} = \frac{\sigma_f'}{E} (2N_f)^b + \epsilon_f' (2N_f)^c \tag{4}$$

where  $2N_f$  is the number of reversals to failure,  $\sigma_f'$  and  $\epsilon_f'$  are the fatigue strength and the fatigue ductility

coefficients, respectively, approximately equal to the true fracture strength and the true fracture strain. The constants  $b$  and  $c$  are the fatigue strength and fatigue ductility exponents, respectively. Their values are seen in Table 6 (Kim et al., 2002).

The transition life is obtained from (4) by putting the elastic and plastic parts of the strain amplitudes equal. The result is given by Equation (5):

$$2N_t = \left( \frac{\epsilon_f' E}{\sigma_f'} \right)^{\frac{1}{b-c}} \tag{5}$$

From the values of Table 6 one obtains:

$$2N_t = 1565$$

Taking the total strain curve from Figure 8 and approximating the slopes at low and high numbers of cycles to failure, the transition life taken from the crossing of the lines is estimated to  $2N_t = 1300$ . This is shown in Figure 9 and 10 is the result of a finite element simulation of fatigue using the finite element program Ansys as

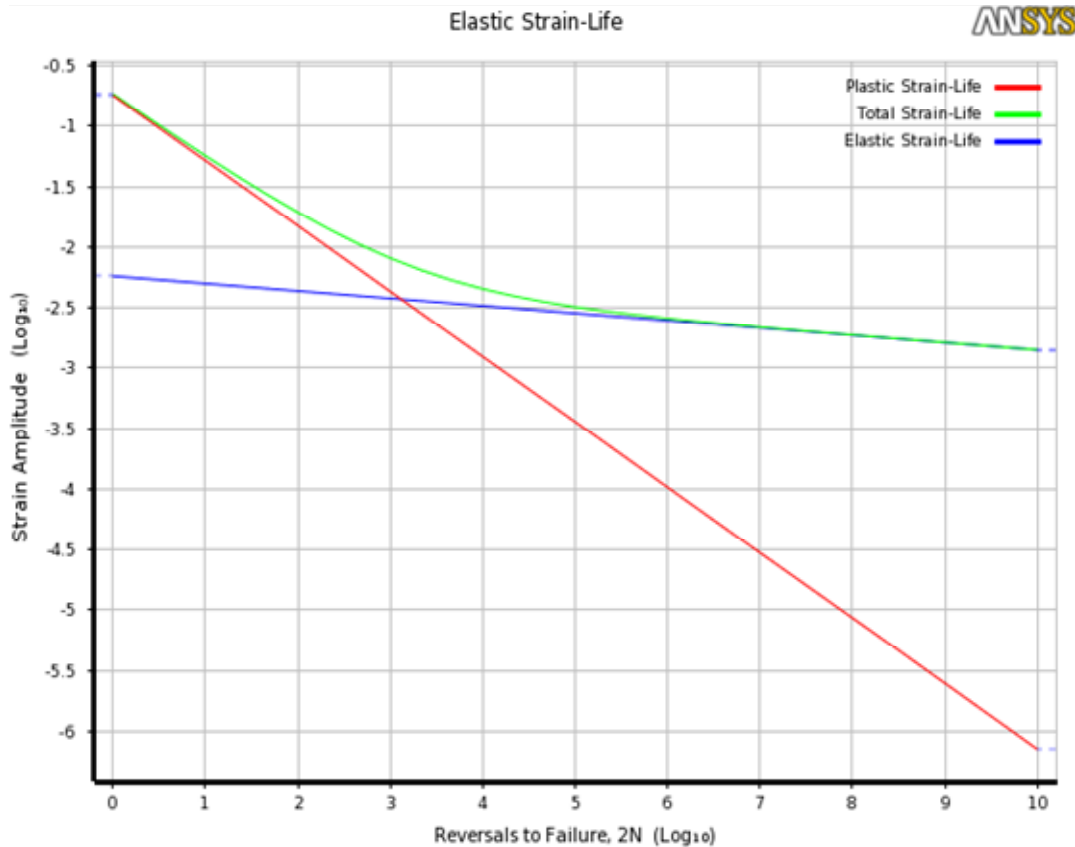


**Figure 10.** Total, elastic and plastic strain amplitudes as functions of reversals to failure from Ansys analysis.

described subsequently. The estimate from Figure 10 gives  $2N_t = 1270$ . These estimates compose well. The value from Equation (5) is somewhat higher, probably due to the somewhat imprecise values of the constants in Table 6, adopted from steel with the same carbon content as SS-1672.

### **FEM model**

Numerical simulation of the dynamic behavior of the sample is better step to predict the building model and understanding the objectives components is used in service during fatigue is performed with the finite element program Ansys and fatigue life analyses by using the fatigue life prediction method in Ansys (Smolnicki et al., 2007). The material constitutive model is the same as for the indentation simulation with values from Table 2. The element type is 8 node linear hexagonal and tetrahedron elements, and 5280 elements were used. The model is seen in Figure 11.

Figure 11 shows the fatigue life distribution in the specimen under maximum tension with a load of 21 kN. The image show that small regions within the measuring

length close to the specimen ends connections have slightly lower fatigue life than the specimen center. This also composes to the actual fracture site at Low Cycle Fatigue (LCF). From the simulation, a minimum life of approximately 570 cycles is obtained. This also composes to the actual number of cycles to failure of approximately 550 cycles at a load level of 21.9 kN (Table 5).

### **Microstructure analysis**

The micrographs in Figures 12 and 13 are taken in a SEM with magnifications 876 and 2000 X, respectively. Before heat treatment it is observed from Figure 12 that the phases which are present are ferrite ( $\alpha$  - iron) and pearlite ( $\text{Fe}_3\text{C} + \alpha$  - iron). In Figure 13, taken after hardening heat treatment at 850°C, the martinstic phase is clearly distinguished.

Martinsite is a distorted body-centered  $\gamma$ -iron with an additional carbon atom in its middle, this causes internal stresses that make this structure very hard but brittle and by heat treatments with the temperatures as 250, 450, 650°C other structures similar to Martensite produced,

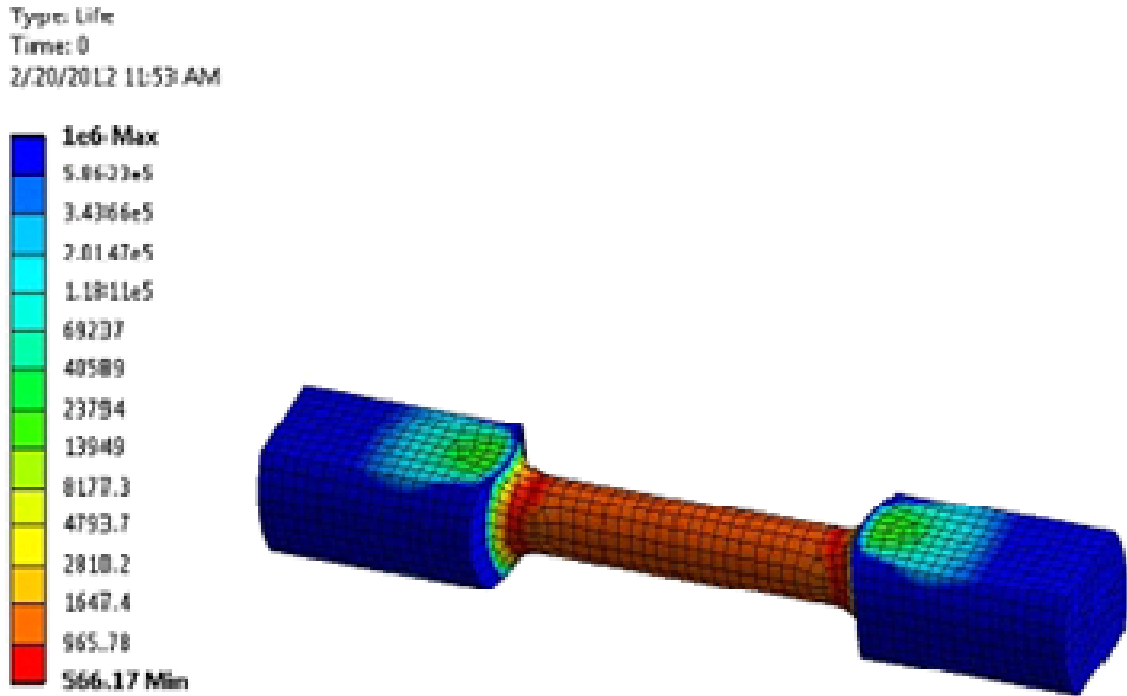


Figure 11. Life distribution in the fatigue specimen from FEM simulation.

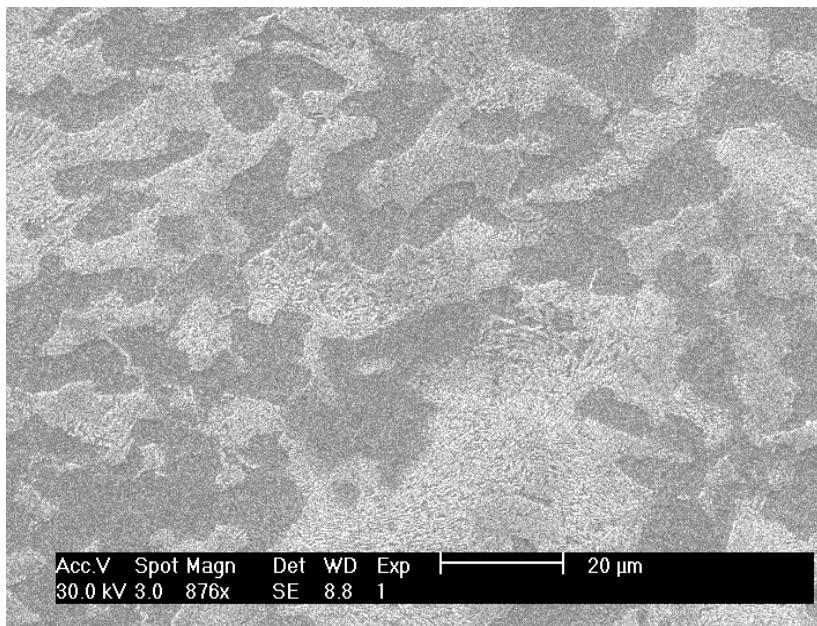
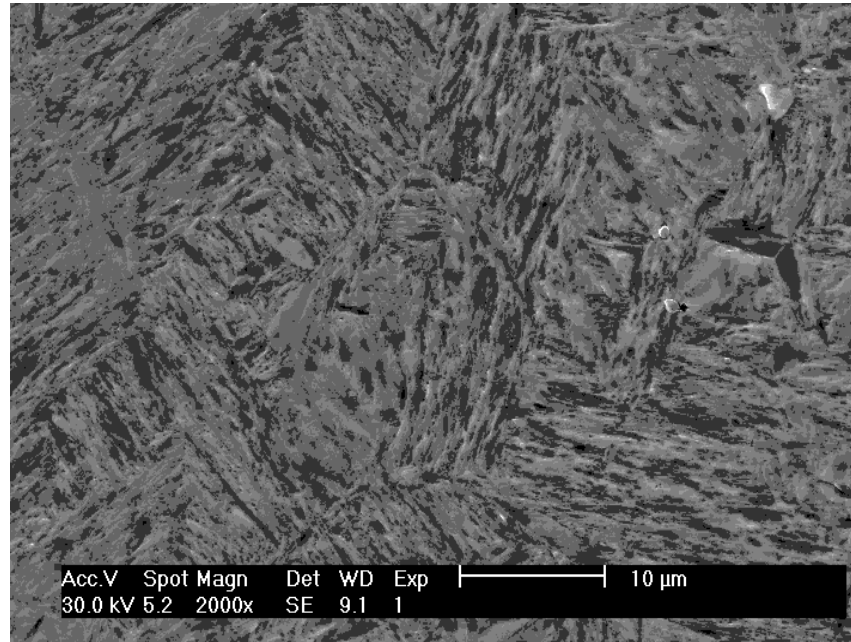


Figure 12. Pearlite (Fe<sub>3</sub>C+α-iron) microstructure at 876 X magnification factor.

such as Trostite and Sorbite, respectively were shown in Figure 14, that are not as hard, but more ductile at grains with plastic formation and composition of striation. Figure 14 Show the tempered Martensite with 250 and 650°C, respectively.

### Fractography

Fractography studies of specimens failed under both Low Cycle Fatigue (LCF) and high cycle fatigue (HCF) conditions were performed. Pictures of the fracture



**Figure 13.** Martensite microstructure at 2000X magnification factor.

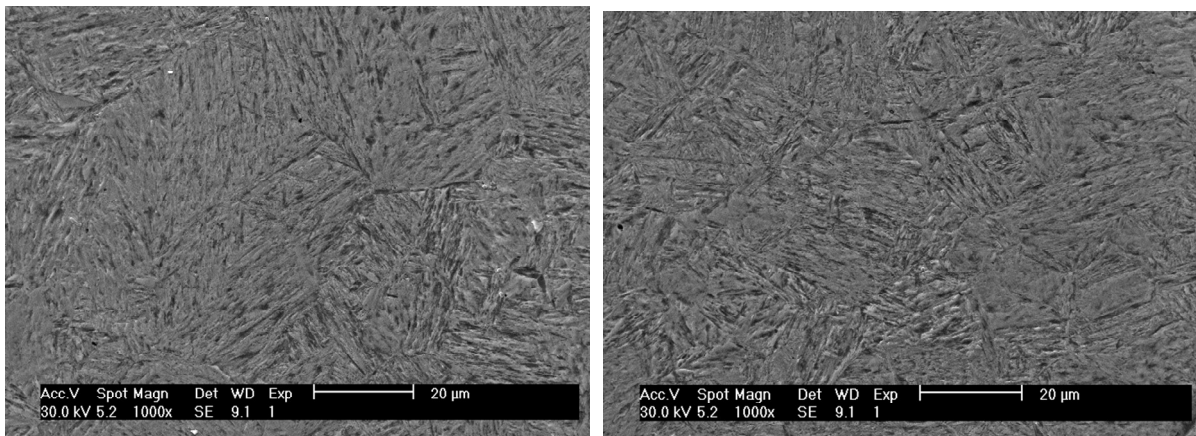


**Figure 14.** Tempered Martensite (Troostite and Sorbite) microstructure at 2000 X magnification factor at 250 and 650°C, respectively.

surfaces were taken in a SEM at magnifications 1600, 3200 and 3206 X. The results are seen in Figure 15 (LCF) and 17 (HCF). The specimen in Figure 15 was loaded by 11.6 MPa and the specimen in Figure 16 by 19.6 MPa (Table 5). From the graphs in Figure 15, in the LCF region at magnifications 1600 and 3206 X, ductile dimples and a number of micro voids are observed.

From the graphs in Figure 15, in the HCF region at magnifications 1600 and 3200 X, brittle cleavage fracture is seen as well as bright or white lines in the facets, which show how the grains have split by cleavage during the fatigue fracture.

## Conclusion

An investigation of the characteristics of steel SS-1672 has been performed. For the martensite phase, it is observed that the hardness decreases with increasing tempering temperature due to the increasing ductility of the tempering martensite phase induced by the tempering, increasing the resistance of the material to fracture and relieving the internal stresses. An Abaqus simulation predicts the effective plastic zone to extend 0.94 mm along the symmetry line when the yield stress is set equal to the von Mises stress.

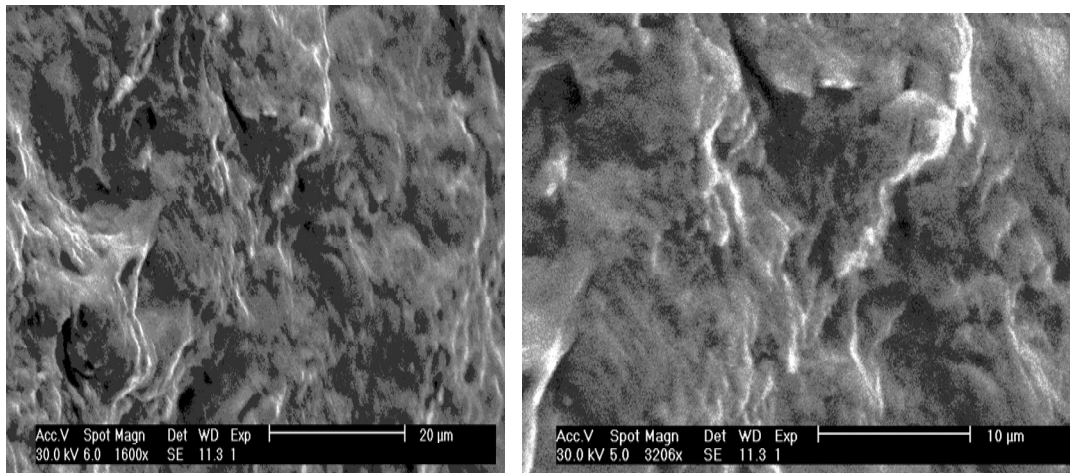


**Figure 15.** Fracture surface microstructure of a LCF region sample with magnifications 1600 and 3200 X.

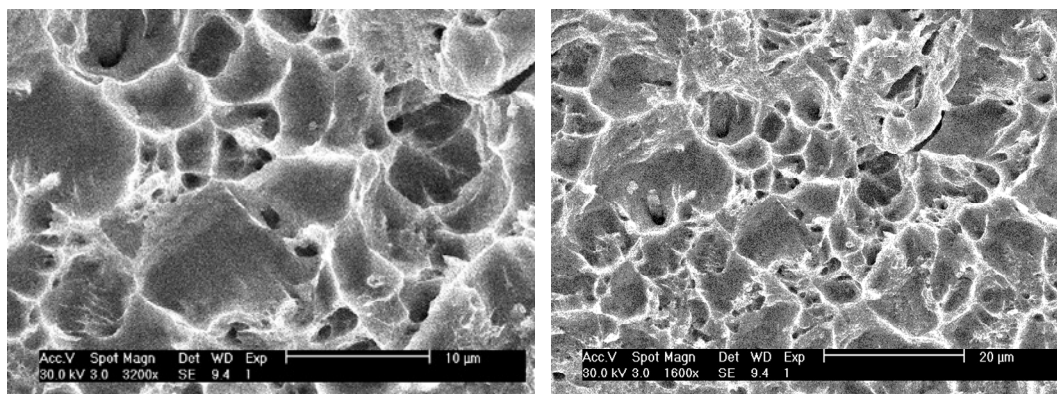


**Figure 16.** Fracture surface microstructure of a HCF region sample with magnifications 3200 and 1600 X.

From the simulation a minimum life of approximately 570 cycle is obtained. This also compasses to the actual number of cycles to failure of approximately 550 cycles at a load level of 21.9 kN. The transition life estimated from the crossing of the lines of slopes at high and low number of cycles to failure is lower than when using the Morrow relation, probably due to the lack of some parameter influences such as the ductility exponent in the Morrow relation.

With the finite element program Ansys, it was shown that small regions close to the ends of the fatigue specimens have slightly lower fatigue life than in the specimen center. The stress in these regions increases due to the shape of the structure.

The specimens failed under both LCF and HCF conditions. The LCF region showed ductile dimples and a number of micro voids and for the HCF region brittle cleavage fractures and bright or white lines in the facets

were observed, indicating how the grains have undergone cleavage.

## ACKNOWLEDGEMENTS

The authors would like to thank everyone who so kindly responded to my request for fatigue and morphology tests throughout the research. Special thanks go to Zivorad Zivkovic, Ling Chen and Behrouz Afzali Far. I greatly acknowledge the support from the Divisions of Material Science and Mechanics at Lund University, Sweden.

## REFERENCES

ASM Handbook (1996). Fatigue and fracture. ASM International, 19: 1057, ISBN: 978-0-97170-385-9.

- Balbi M, Avalos M, El Bartali A, Armas I A (2009). Microcrack growth and fatigue behavior of a duplex stainless steel. *Int. J. Fatigue* 31:2006-2013.
- Chiu PK, Weng KL, Wang SH, Yang JR, Huang YS, Fang J (2005). Low- cycle fatigue-induced martensitic transformation in SAF 2205 duplex stainless steel. *Mater. Sci. Eng. A* 398:349-359.
- Eric PA (2006). *Stainless Steel in the Food & Beverage Industry*. First edition, Materials and applications series, 7, Euro Inox. Fagersta datablad for steel, Fagersta Bruks AB, Fagersta, Sweden, (1962).
- Handbook in Solid Mechanics (2008). Department of Solid Mechanics, KTH, Stockholm, Sweden, 3 ed., pp:372-373
- ISO (2002). *Metallic materials - instrumented indentation test for hardness and material parameters. Part 1: test method*, Geneva, Switzerland, 14577-1.
- Jaykant GU (2009). "Mechanical and Wear Properties of Carburizes Mild Steel Samples. Master thesis Roll No. 207ME 207, Department of Mechanical Engineering, national Institute of Technology, Rourkela, Orissa, India.
- Kim KS, Chen X, Han C, Lee HW (2002). Estimation methods for fatigue properties of steels under axial and tensional loading. *Int. J. Fatigue*, 24:783-793.
- Ottosen N, Ristinmaa M (2005). *The mechanics of constitutive modeling*. First edition, ISBN: 0-008-044606-X, pp. 279-285.
- Robert LN (2005). *Mechanic Design: An Integrated Approach*. 3ed, Prentice- Hall.
- Smolnicki T, Rusiński E, Karliński J (2007). FEM modelling of fatigue loaded bolted flange joints *J. Achiev. Mater. Manuf. Eng.* 22(1):69-71.
- Suresh S (2001). *Fatigue of Materials*. Second edition Cambridge University press,
- Yung LI, Jwo PA, Richard BH, Mark EB (2005). *Fatigue Testing and Analysis. Theory and fatigue practice*, Elsevier's Science & Technology rights Department in Oxford, UK.